Probability currents and entropy production in nonequilibrium lattice systems

György Szabó,[1] Tânia Tomé,[2] and István Borsos[1]
[1]*Research Institute for Technical Physics and Materials Science, P.O. Box 49, H-1525 Budapest, Hungary*
[2]*Instituto de Física, Universidade de São Paulo, Caixa Postal 66318, 05314-970 São Paulo, SP, Brazil*
(Received 1 December 2009; revised manuscript received 3 March 2010; published 6 July 2010)

The structure of probability currents is studied for the dynamical network after consecutive contraction on two-state, nonequilibrium lattice systems. This procedure allows us to investigate the transition rates between configurations on small clusters and highlights some relevant effects of lattice symmetries on the elementary transitions that are responsible for entropy production. A method is suggested to estimate the entropy production for different levels of approximations (cluster sizes) as demonstrated in the two-dimensional contact process with mutation.

DOI: 10.1103/PhysRevE.82.011105 PACS number(s): 05.70.Ln, 05.50.+q

I. INTRODUCTION

A dynamical network theory was developed by Schnakenberg [1] to study the behavior of nonequilibrium systems that can be described by a master equation

$$\partial_t P_i(t) = \sum_{j=1}^{N} [-w_{ij}P_i(t) + w_{ji}P_j(t)], \tag{1}$$

where $P_i(t)$ denotes the probability of the microscopic state i at time t $[0 \le P_i(t) \le 1,\ i=1,2,\ldots,N,\ \Sigma_{i=1}^{N} P_i(t)=1]$ and w_{ij} is the transition probability per time from state i to state j. The number N of the microscopic states is finite, however, the limit $N \to \infty$ can also be investigated without principal difficulties. The master equation (1) can be graphically represented by a graph G with N nodes where each node refers to a microscopic state and the edges connect the nodes i and j if there exists microscopic transition between the corresponding states. Along the edges we can define the probability current,

$$K_{ij} = -w_{ij}P_i(t) + w_{ji}P_j(t) \tag{2}$$

expressing the difference in the frequency of transitions from state i to j and backward within a unit time. The definition ensures that $K_{ij}=-K_{ji}$ and the assumption of $K_{ii}=0$ for all i simplifies the subsequent notation where the master equation obeys the following form:

$$\partial_t P_i(t) = \sum_{j=1}^{N} K_{ij}. \tag{3}$$

In many cases the system has a unique stationary state $P_i^\star = \lim_{t\to\infty} P_i(t)$ where the stationary value of the probability current satisfy a condition

$$\sum_{j=1}^{N} K_{ij}^\star = 0 \tag{4}$$

resembling the Kirchhoff's current law (henceforth KCL) for each nodes (states) [2]. If the condition of detailed balance is satisfied then $K_{ij}^\star=0$ for all $i \neq j$. The stationary state, however, can exist in the presence of probability currents between the microscopic states if they form a suitable current loop structure, too. Several relations between the stationary state, the structure of the possible probability currents, the entropy production and phase transition are already discussed in the literature [1,3–7]. This mathematical background is related directly to the random walks on the corresponding network [8]. Zia and Schmittmann [9,10] suggested using the structure of probability current loops to classify nonequilibrium systems and/or steady states. A particular structure of probability currents was investigated by Lecomte *et al.* [11] who studied a two-temperature Ising model.

Now, applying the above mathematical framework we study two-state, nonequilibrium lattice systems where the consecutive elementary processes allow changes only at one randomly chosen site of a square lattice. Instead of investigating the whole (M-particle) system our attention will be concentrated on a set of unified states where each element represents a configuration occurring on a small (n-site) cluster of sites. This approach is used successfully for the cluster variation method [12,13] and also for the dynamical cluster techniques when studying nonequilibrium systems [14–16]. As mentioned above the corresponding cluster configuration probabilities can be derived by summing the probability of (M-site) microscopic states over the states of site variables residing outside of the given cluster. At the same time this summation is equivalent to a series of graph contraction unifying nodes along those edges of the dynamical graph that represent transitions at site variables being outside of the n-site cluster. After the consecutive contractions of the dynamical graph the probability currents (along the contracted dynamical graph) obey a structure exhibiting some basic symmetries. Here we demonstrates that these symmetries can even yield zero probability currents along all the edges of the small (contracted) dynamical graph despite the breaking of detailed balance at the level of microscopic (M-site) description. It is found, furthermore, that the relevant features of the structure of probability currents occur when choosing a sufficiently large cluster consisting of a focal site and its neighbors. In the latter cases we can give a series of estimations (with an increase of neighborhood) for the entropy production per sites for those nonequilibrium lattice systems where unidirectional transitions are forbidden between two microscopic states.

It is emphasized that the determination of entropy production quantifies the deviation from the detailed balance for many nonequilibrium lattice systems, such as the spatial evolutionary games [17], predator-prey models [18], and many others. In the present work the essence of this approach is

described. Its applicability and also the emerging difficulties are demonstrated by studying numerically the two-dimensional contact process [19,20] in the absence and presence of a weak (symmetric) mutation.

II. MATHEMATICAL FRAMEWORK

We consider nonequilibrium systems on a square lattice with $M=L\times L$ equivalent sites under periodic boundary conditions to ensure the symmetries (e.g., translation, reflection, and rotation). Each equivalent site x of the system has two possible states, namely, $s_x=0$ or 1 for $x=1,\ldots,M$. Using the formalism of the Ising model the microscopic state is defined by an M-dimensional vector of the two-state variables, $\mathbf{s}=(s_1,\ldots,s_M)$. These microscopic states (henceforth configurations) were labeled from $i=1$ to $i=N=2^M$ in the previous section. The probability of a given configuration $\mathbf{s}$ is denoted as $Q(\mathbf{s})$.

Our investigation will be focused on those systems where the evolution is governed by consecutive elementary steps modifying the state only at one site chosen at random. Examples are the kinetic Ising model with Glauber dynamics [21] and its nonequilibrium versions [22], the majority vote model [5,23,24], spatial evolutionary games [17], etc. Counterexamples are the kinetic Ising (or lattice gas) models with Kawasaki dynamics [25], driven lattice gases [26], asymmetric exclusion process [27], and so on, where two neighboring state variables change simultaneously.

For the present systems the quantities $W_0^{(x)}(\mathbf{s})$ and $W_1^{(x)}(\mathbf{s})$ describes the transition probabilities for a single site change, namely for $s_x=0\to 1$ and $s_x=1\to 0$ for the given surrounding indicated shortly by $\mathbf{s}$. The corresponding probability currents between these two microscopic states are defined as differences between the transition rates, that is, $K_0^{(x)}(\mathbf{s})=-K_1^{(x)}(\mathbf{s})=W_0^{(x)}(\mathbf{s})-W_1^{(x)}(\mathbf{s})$. Evidently, these currents satisfy the KCL in the stationary state.

The dynamical graph G_M of these two-state lattice systems can be well represented by an M-dimensional hypercube with nodes defined by the vector $\mathbf{s}$. For the present dynamical rules the parallel edges of hypercube refer to transitions $s_x=0\to 1$ and $s_x=1\to 0$ for the same site x.

For any realistic system size the dynamical graph G_M becomes vast that causes difficulties in the network analysis. At the same time some basic features of the dynamical graph (structure of probability currents) become obvious when reducing the graph size via consecutive elementary contractions. During an elementary contraction we unite pairs of nodes connected by parallel edges. In other words, the d-dimensional hypercube is transformed into a $(d-1)$-dimensional hypercube by eliminating one of the site variables. Evidently, this process involves the elimination of edges indicating the transitions at the given site. In addition, the unification of nodes is accompanied by the unification of edges with a summation of the corresponding probability currents. As a result, on the contracted dynamical graph G_{d-1} the resultant probability currents satisfy the KCL, too. Repeating this contraction one can arrive to a situation when only a few site variables characterize the system and the dynamical graph becomes easy to survey.

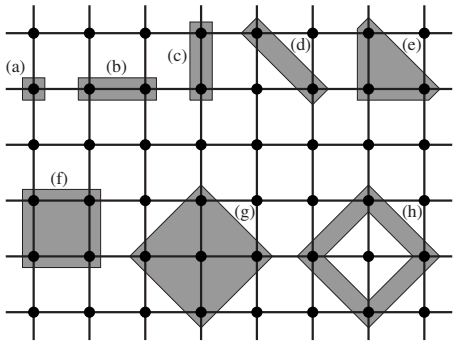

FIG. 1. Several types of clusters on which the dynamical network of configurations are studied. Notice that the larger four-site cluster (h), obtained by neglecting the focal site of the five-site cluster (g), possesses the same symmetries as the smaller one (f).

Henceforth we study the resultant probability currents when the sites form compact clusters as shown in Fig. 1. Within this approach the probability of the configuration $\mathbf{s}_n=\{s_1,\ldots,s_n\}$ on an n-site cluster is denoted in a simplified way by $q_n(\mathbf{s}_n)$. For the present analysis the shape and orientation of the n-site clusters are not relevant therefore now these features are not specified in our notation. The configuration probabilities are positive (or zero) quantities and satisfy the condition of normalization, namely $\Sigma_{\mathbf{s}_n}q_n(\mathbf{s}_n)=1$. Besides it the configuration probabilities on different clusters are related to each other by the so-called compatibility conditions detailed in previous papers [12–14,17]. The corresponding transition rate for $s_x=0\to 1$ $(s_x\in\mathbf{s}_n)$ in the case of n-site configurations is given as

$$W_0^{(x)}(\mathbf{s}_n)=\sum_{s_y\notin\mathbf{s}_n}W_0^{(x)}(\mathbf{s}) \tag{5}$$

and similar summation defines the opposite transition rates $W_0^{(x)}(\mathbf{s}_n)$ as well as probability currents [e.g., $K_0^{(x)}(\mathbf{s}_n)=W_0^{(x)}(\mathbf{s}_n)-W_1^{(x)}(\mathbf{s}_n)$] for the reduced neighborhood $\mathbf{s}_n$.

Features of the resultant probability current structure will be illustrated by considering several examples below. For the sake of simplicity the analyzes are begun with the smallest (one-site) cluster and then we choose larger and larger cluster to demonstrate the main features.

It is emphasized that the transition rate between two n-site configurations (and also the configuration probabilities) can be numerically determined during the Monte Carlo simulations by recording the events for each possible transitions independently of the value of x for a given set of local constellation $(\mathbf{s}_n)$. The accuracy of the numerical analysis is improved significantly by averaging over a long run time and all the sites (due to the translation invariance).

In most of the explanations and numerical examples we will use the convenient context of the contact process [19,20] exemplifying all the relevant phenomena characteristic to a large set of models mentioned above. This model was developed to describe the spreading of infection among individuals located on the sites x of a square lattice. The state variable $s_x=0$ $(s_x=1)$ refers to healthy (infected) individual at site x. The spatiotemporal evolution of the healthy or infected state of individuals are governed by infection $(s_x=0$

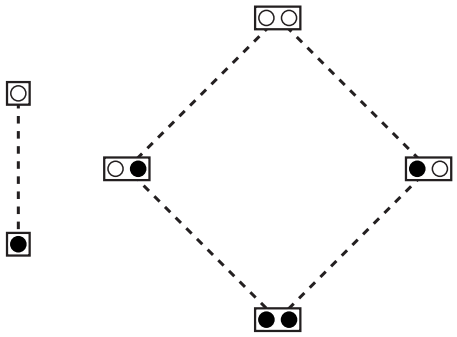

FIG. 2. Dynamical network for the one-site (left) and two-site (right) configurations. Dashed lines refer to detailed balance between the connected configurations where the local states 0 and 1 are denoted by empty and closed circles.

$\rightarrow s_x=1$) and recovery ($s_x=1\rightarrow s_x=0$). On the one hand, the healthy individuals can be infected by their neighbors with a probability $dt\lambda n_x^{(i)}/z$ within an infinitesimally short time dt time, where $n_x^{(i)}$ denotes the number of infected neighbors of site x, z is the total number of neighbors, and λ describe the strength of infection within a time unit defined by the speed of recovery. On the other hand, the infected individuals can become healthy with a probability dt that is the recovering defines the time unit in the system. The system is started from a random initial state and after many elementary steps $\rho=\langle\Sigma_x s_x\rangle/M$ portion of the whole population are infected in the final stationary state. When increasing λ this system exhibits a phase transition (belonging to the directed percolation universality class [20]) at a critical value of λ from the absorbing state ($\rho=0$) to the active state $0<\rho<1$, and $\rho\rightarrow 1$ if $\lambda\rightarrow\infty$.

For the one-site approximation ($n=1$) the stationary state of the system is characterized by only two configurations and the corresponding configuration probabilities, $q_1(1)=\rho$ and $q_1(0)=1-\rho$. Evidently, the frequencies of the transition from state 0 to 1 and backward should be equivalent in the stationary state, that is, the corresponding dynamical graph G_1 consists of two nodes connected by an edge with a zero probability current between the one-site configurations 0 and 1.

For the two-site cluster approach the quantity $q_2(s_1,s_2)$ gives the probability of (s_1,s_2) configuration on two neighboring sites independently of the position and orientation of the 2×1 cluster. These quantities satisfy the so-called compatibility conditions [14], that is, $q_1(s_1)=\Sigma_{s_2}q_2(s_1,s_2)=\Sigma_{s_2}q_2(s_2,s_1)$. Due to the compatibility conditions (and normalization) the four configuration probabilities can be characterized by only two parameters. As the consecutive elementary processes allow a change only at one of the two sites therefore the dynamical network of the four states forms a loop as illustrated in Fig. 2.

For the dynamical network G_2 the KCL allows the existence of a probability current loop with a constant current J. However, in the present systems the probability currents from the configuration (0,0) to (0,1) or to (1,0) are equivalent because of the symmetries. Consequently, the probability current vanishes ($J=0$) between the connected configurations along the whole loop. This means that the deviation from the detailed balance is forbidden within the framework of two-site (pair) approximation, too.

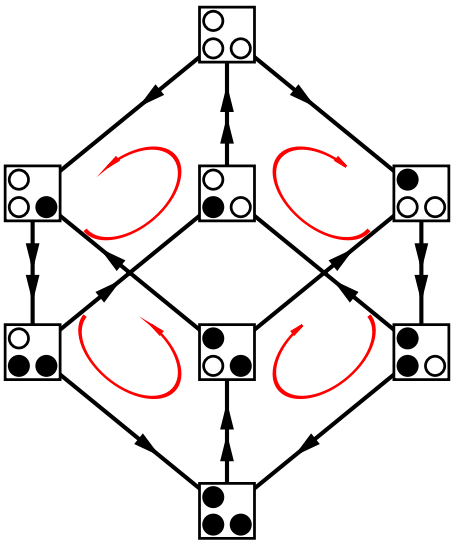

FIG. 3. (Color online) Two-dimensional projection of the "cubic" dynamical network for the three-site configurations. Red arcs denote four, nonvanishing probability current loops with equal strength J_1. The single (and double) arrows along the edges refer to probability currents with a strength J_1 (and $2J_1$).

Figure 3 illustrates that the dynamical network G_3 can be represented by a cube for the three-site configurations. More precisely, the corresponding three-dimensional (cubic) dynamical network can be given by the nodes at the three-dimensional vector positions (s_1,s_2,s_3) where $s_1,s_2,s_3=0$ or 1 [here the label 2 refers to the focal site having two nearest neighbors within the three-site cluster (see cluster (e) in Fig. 1], and the edges of the cube demonstrate the possible elementary transitions. For the sake of illustration this cube is projected to a two-dimensional plane spanned by the unit vectors $\mathbf{e}_y=-1/\sqrt{3}\cdot(1,1,1)$ and $\mathbf{e}_x=1/\sqrt{2}\cdot(1,0,-1)$. Using this projection one can distinguish four vertical levels in such a way that the number of infected sites increases by one from top to bottom. The interpretation of the results for the contact process is helped by recognizing that infection (recovering) occurs along the edges downward (upward).

In such a network the KCL and symmetries allow four, nonvanishing probability current loops as denoted by red arcs on the given faces of the cube (see Fig. 3). The strengths of the upper (lower) two current loops are equivalent because of the rotation symmetry. The equivalence between the upper and lower loop currents can be justified by contracting the dynamical network G_3 into G_2 that gives a relationship between the two- and three-site configuration probabilities, that is, $q_2(s_1,s_2)=\Sigma_{s_3}q_3(s_1,s_2,s_3)=\Sigma_{s_3}q_3(s_3,s_2,s_1)$. In the present case the contraction means the unification of configuration pairs, for example, the three-site configurations $(s_1,s_2,0)$ and $(s_1,s_2,1)$ are united into the two-site configuration (s_1,s_2). In the graphical representation (see Fig. 3) this mathematical manipulation is equivalent to the unification of two opposite faces of the cubic network into one square [shown in Fig. 2(b)]. During the contraction the probability currents of the unified edges are added algebraically. Consequently, the

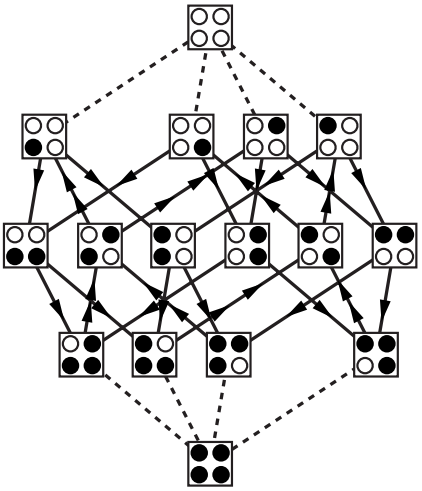

FIG. 4. Dynamical network of the four-site configurations. The arrows and double arrows indicate the direction and strength J_1 and $2J_1$ of probability current. Dashed lines refer to zero current (detailed balance) as shown also in Fig. 2.

probability loop current for the two-site configurations can vanish if all the four probability current loops of the three-site configurations are equivalent. In fact, the KCL allows the existence of a fifth probability current loop that can be located on one of the "loop-free faces" of the cube. The corresponding current loop survives the contraction of the graph along the vertical edges. The latter contraction is related to the compatibility condition $q_2'(s_1,s_3)=\Sigma_{s_2}q_3(s_1,s_2,s_3)$ where $q_2'(s_1,s_3)$ is the configuration probability on a pair of sites being second neighbors. However, the probability currents in the corresponding dynamical graph become zero because of the same reasons discussed for the case of nearest neighbors.

Notice that all the four equivalent probability current loops involve the same four microscopic steps illustrated in Fig. 2. As one of the sites remains unchanged along the indicated current loops the remainder two-site configurations can transfer to each other as defined in Fig. 2. In the present case, however, the probability current is not prevented by symmetries due to the symmetry breaking at the additional (third) site. Here it is worth mentioning that all the probability loop currents vanish on triangular lattices because of the equivalence of sites forming a regular triangle. In other words, one cannot observe the breaking of detailed balance when considering the possible transitions between the configurations on a regular triangle.

In agreement with the above results the equivalence between the four probability loop currents can also be derived by contracting the dynamical network G_4 of the four-site configurations into the "cubic" network G_3. First we emphasize that the dynamical network G_4 is equivalent to a four-dimensional hyper cube with edges defining elementary transitions between the 16 configurations as indicated in Fig. 4. For the two-dimensional illustration of the given dynamical network we used the same trick as above. Namely, the four-dimensional hyper cube is projected to a plane where the vertical axis is parallel to the diagonal from node (1,1,1,1) to (0,0,0,0). The direction of "horizontal vector" is chosen to have equidistant spatial distribution of nodes (configurations) with two "1"s and "0"s in the middle level.

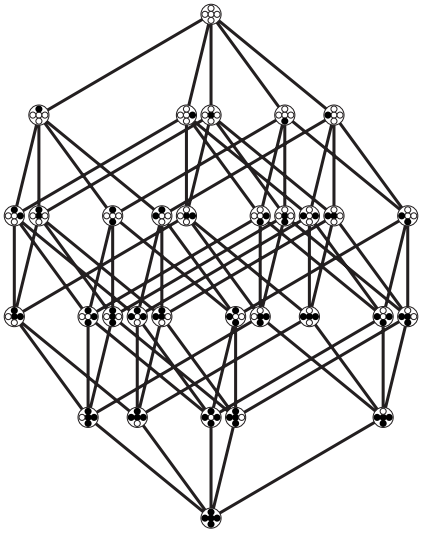

FIG. 5. Dynamical network of the five-site configurations is represented by a suitable two-dimensional projection of the five-dimensional hypercube.

Figure 4 shows that from the "bottom" and "top" configurations [i.e., from (1,1,1,1) and (0,0,0,0)] all the four probability currents (see dashed lines) are zero due to the KCL and symmetries as mentioned above. For the simplest probability current loop structure all the other nodes belong to two of eight (nonvanishing) equivalent probability current loops consisting of four edges. It is emphasized that for the given circuit structure the KCL can be satisfied by introducing 17 independent loop currents, however, 9 of them are suppressed by the symmetries. The probability current loops are not illustrated in Fig. 4. Instead of it, only the direction and the strength (J_1 or $2J_1$) of probability currents are indicated by arrows and double arrows in Fig. 4.

The mentioned four-edge probability current loops can be transformed into each other by applying the lattice symmetries. Consequently, these loops have some common features. Namely, along these loops only two (nearest-neighbor) site variables can change following the scenario represented graphically in Fig. 2(b) while on the other two sites the configuration (0,1) [or (1,0)] is fixed and provides a symmetry breaking that is necessary for the appearance of a loop current with a finite strength J. In other words, the analysis of the four-site configurations is capable to account only one type of microscopic mechanisms yielding twisted (entangled) probability current loops in these systems.

Finally we briefly study the dynamical network (G_5) of the five-site cluster [(g) in Fig. 1] to illustrate several features that cannot occur on the above discussed clusters. Figure 5 makes clear that the detailed analysis becomes difficult because of the large number of nodes and edges.

Notice that in this graphical representation the state of the central site varies along the vertical edges. For example, the transition from the totally healthy state to the infected central site is indicated by the vertical (central) edge from the top node in Fig. 5. Evidently, the four additional transitions from the top node are equivalent and have a probability current with a strength of one quarter of the central one (with an opposite sign to satisfy KCL on top node).

The central (vertical) edge from the top node in Fig. 5 has an additional curiosity. Namely, it is a unidirectional transition because along this edge only the upward transition is allowed in the two-dimensional contact process. Similar unidirectional edges will occur for larger dynamical graphs where the local condition (four healthy sites around the focal one) prohibits the infection of the focal site while the spontaneous recovery is allowed for the same neighborhood.

As emphasized above the four-site clusters (f) and (h) exhibit the same symmetries. The corresponding dynamical graph on the cluster (h) can be obtained by contracting the graph of Fig. 5 along the vertical edges. Consequently, on cluster (h) one can expect a probability current structure similar to those discussed in the case of cluster (f). The only difference is the strength J_2 characterizing transitions between configurations on two second-neighbor sites.

The above investigations imply the possibility of similar investigations on larger clusters. The investigated cluster may even involve the whole system when the corresponding dynamical graph G_M is represented by an M-dimensional hypercube on the analogy of dynamical graphs on a small cluster (the main topological features of the d-dimensional hypercubes are summarized in Appendix). Evidently, one can get more and more accurate (and detailed) pictures about the microscopic processes when increasing the size of cluster. In order to demonstrate the complex structure of the probability currents we numerically study the contact process in the next section.

III. NUMERICAL RESULTS

To quantify the magnitude of probability currents in the two-dimensional contact process we have performed Monte Carlo simulations under periodic boundary conditions on square lattice with $M=L\times L$ sites. In these simulations the system is started from a random initial state and after a suitable thermalization time t_{th} we have determined the value of ρ, the transition probabilities and currents (J) between several local configurations on the clusters indicated in Fig. 1 by averaging over a sufficiently long sampling time t_s. In most of the simulations we set $L=400$, $t_s=t_{th}\approx 10^4$, however, in the close vicinity of the critical transition [where $\rho\approx(\lambda-\lambda_c)^{\beta}$, $\lambda_c=1.6488(1)$, $\beta=0.583(4)$] we used larger sizes and longer times to suppress the undesirable effect of diverging fluctuations and relaxation time [20].

Figure 6 illustrates the probability currents J_1 characterizing the strength of the corresponding loop current for different values of birth-death rate (λ) in G_4 representing four-site configurations (and transitions) on cluster (f) of Fig. 1. Evidently, the same $J_1(\lambda)$ values are found for G_3 shown in Fig. 3. Besides it, in this plot we also illustrate the λ-dependence of J_2 characterizing the strength of currents in another four-site subsystem (G_4') on the cluster (h) of Fig. 1. In agreement with the expectation these currents behave alike, that is, both currents vanish when λ approaches λ_c or goes to infinity. Notice, furthermore, that $|J_1|\gg|J_2|$ in the whole range of λ. The latter feature indicates that the nearest neighbors influence the deviation from the detailed balance more efficiently. It is also found that J_2 decreases faster when $\lambda\to\infty$.

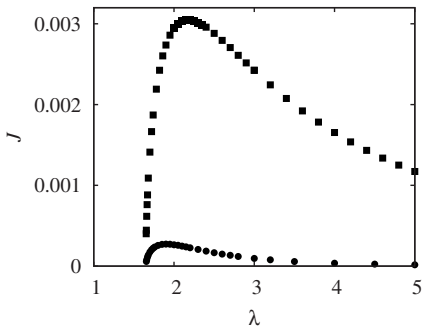

FIG. 6. Monte Carlo results for the probability currents J_1 (closed squares) and J_2 (bullets) versus λ for the dynamical graphs on the four-site clusters (f) and (h) (shown in Fig. 1) in the two-dimensional contact process.

In order to have a more accurate picture about the vanishing of the probability currents J_1 and J_2 the latter quantities are also plotted as a function of ρ in Fig. 7. The MC results show clearly that these currents vanish linearly with ρ when approaching the critical point. This means that both J_1 and J_2 exhibit the same power law behavior characterizing the decrease of ρ in the vicinity of the critical transition (for details see Refs. [19,20]). On the contrary, it is found that J_1 becomes proportional to $(1-\rho)^2$ if $\lambda\to\infty$ when ρ tends to 1. The different behaviors can be related to the fact that the state $\rho=0$ is an absorbing one, that is, the community remains healthy for ever in the absence of infected individuals. In the opposite case ($\rho=1$), however, any infected sites can recover and these solitary healthy sites will be infected again within a short time while the neighborhood remains unchanged.

In the above examples the probability currents are always obtained by averaging (summarizing) over many configurations including states in the neighborhood of the focal site where the local state is changed.

Figure 8 illustrates the λ-dependence of the probability currents between the states $s_x=0$ and $s_x=1$ at fixed configurations on the nearest neighbor sites when summing up all the contributions coming from any other local states. In fact these probability currents $K_0^{(x)}(\mathbf{s}_5)$ occur along the vertical edges of the dynamical graph G_5 plotted in Fig. 5.

Due to the above mentioned symmetries we can distinguish only six different values of the probability currents

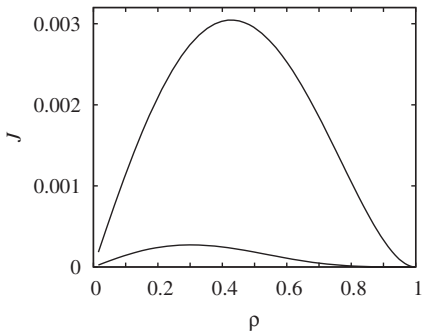

FIG. 7. Probability currents J_1 (upper curve) and J_2 (lower curve) versus the density ρ of infected sites for the contact process on a square lattice. The statistical error is comparable with the line thickness.

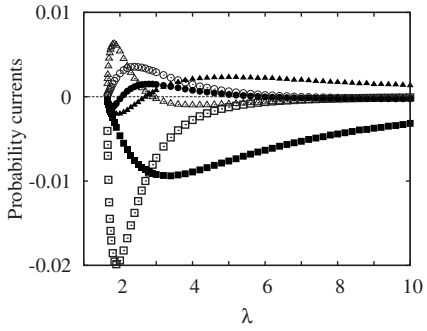

FIG. 8. Probability currents $K_0^{(x)}(\mathbf{s}_5)$ as a function of λ for the transition of the focal site from $s_1=0$ to $s_x=1$ at all the possible configurations on the neighboring four sites. Open squares (closed circles) denote the MC data when all the neighboring states are 0 (1). Analogously, open (closed) triangles represent data when three local states are 0 (1) in the neighborhood. Two types of circles refer to the two cases when two-two ones and zeros are located on the four neighboring sites.

$K_0^{(x)}(\mathbf{s}_5)$ for the 16 configurations of neighborhood. Evidently, the sum of these 16 probability currents is zero for any values of λ. Notice, that the absolute values of these probability currents exceed significantly the values of J_1 and J_2 obtained by averaging over some constellations. In other words, the opposite effects weaken the averaged values. Furthermore, in the stationary state all the probability currents vanish when λ goes to λ_c or ∞.

IV. ENTROPY PRODUCTION

The nonvanishing probability currents in the stationary state of a nonequilibrium system is related to the entropy production [1,3,4] defined as

$$\Pi = \frac{1}{2}\sum_{i,j}^{N} K_{ji}^{\star} \ln \frac{w_{ij}P_j^{\star}}{w_{ji}P_i^{\star}}, \tag{6}$$

where P_j, w_{ij}, and K_{ji} are defined in Eqs. (1)–(3); $P_j^{\star}$ and $K_{ji}^{\star}$ denote the stationary value of P_j and K_{ji}, respectively. The entropy production can be understood as a relative entropy between the transition probabilities and their time reversal [7]. In the present two-state lattice systems independent transitions from 0 to 1 and vice versa can occur at any sites of the system. Due to the translation invariance these local transitions are equivalent. Consequently, the specific entropy production (Π/M) can be evaluated by summing the contributions of those probability currents where changes occur only at a given site x for all the possible configurations on the rest of sites.

Using the notation of Sec. II the specific entropy production can be described by the following expression:

$$\Pi/M = I = \sum_{s_y, y\neq x} [W_0^{(x)}(\mathbf{s}) - W_1^{(x)}(\mathbf{s})] \ln \frac{W_0^{(x)}(\mathbf{s})}{W_1^{(x)}(\mathbf{s})} \tag{7}$$

being independent of x in the translation invariant lattice systems.

If the evolutionary process is controlled by short range interactions then we can assume that the state s_y of site y located far from x will slightly influence the ratio $W_0^{(x)}(\mathbf{s})/W_1^{(x)}(\mathbf{s})$. In that case the contributions of the given configurations $(s_y=0,1)$ can be summarized as it is happened when evaluating the probability current on a smaller system in the previous section. Repeating these summations (or contractions of dynamical graph) one can arrive to a situation when the averaged transition probabilities (e.g., $W_0^{(x)}(\mathbf{s}_n)$) are considered only a small cluster consisting of n sites. Consequently, the specific entropy production can be approximated by considering only a small neighborhood of x.

In the light of the previous analysis of $W_r^{(x)}(\mathbf{s}_n)$ $(r=0,1)$ one can give an adequate approximation for Π/M when using clusters where the focal site x is surrounded symmetrically by its first, second, and kth neighbors. In the simplest situation, one can derive an approximative formula for the specific entropy production when considering the transition probabilities at the focal site x within the five-site cluster (f) shown in Fig. 1. In that case we take into account only the transitions occurring along the vertical edges of G_5 in Fig. 5. The corresponding approximation is given as $\Pi/M \simeq I_5$ where

$$I_5 = \sum_{s_y \in \mathbf{s}_5, s_y \neq s_x} [W_0^{(x)}(\mathbf{s}_5) - W_1^{(x)}(\mathbf{s}_5)] \ln \frac{W_0^{(x)}(\mathbf{s}_5)}{W_1^{(x)}(\mathbf{s}_5)} \tag{8}$$

and the summation runs over all the configurations on the four nearest-neighbor sites. In fact, the probability currents $K_0^{(x)}(\mathbf{s}_5)$ derived from these transition probabilities were numerically discussed previously (see Fig. 8).

Evidently, the approximation can be improved by choosing larger and larger neighborhood. The efficiency of this approach will be demonstrated later when comparing the MC results for I_5 and I_9 where the latter quantity denotes the approximative results based on the nine-site approach (including the nearest- and next-nearest neighbors around the focal site x) with transition probabilities denoted as $W_r^{(x)}(\mathbf{s}_9)$ $(r=0,1)$.

The above expressions of the entropy production are straightforwardly applicable for those lattice systems where the unidirectional transitions are forbidden, that is, where all transition probabilities are positive $[W_r^{(x)}(\mathbf{s}_n)>0$ for both $r=0$ and 1]. This is not the case of the contact process where the transition $s_x=0$ to 1 is forbidden for all configurations where the four neighboring sites are healthy (0). However, if we introduce mutation in the contact process then the above expressions for the entropy production can be applied.

In order to demonstrate some numerical results henceforth we study a modified contact process where any state s_x can transform into $(1-s_x)$ with a probability μdt within a time dt. Notice, that this extension does not influence the topological features of the dynamical graphs and all the transition rates are increased with a quantity proportional to μ.

A series of MC simulations were performed to determine numerically the transition probabilities $W_r^{(x)}(\mathbf{s}_n)$ at $n=5$ and 9 if $\mu=0.001$ for different values of λ. From these numerical data we could derive approximations (I_5 and I_9) for the specific entropy production as illustrated in Fig. 9.

Due to the mutation this system cannot reach the states where $\rho=0$ or $\rho=1$. In other words, this type of mutation

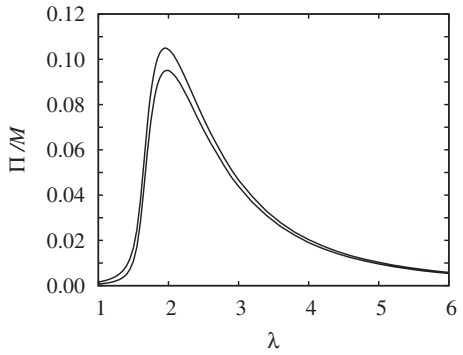

FIG. 9. Approximative results of the specific entropy production *vs*. λ for the contact process with a low mutation rate ($\mu=0.001$) on the square lattice. The upper and lower lines show the results for I_9 and I_5. The statistical errors are comparable with the line thickness.

creates both infected and healthy sites in the system within the whole range of λ. In addition, the critical transition at $\lambda=\lambda_c$ is smoothed [20]. Consequently, the specific entropy production as well as the probability currents differ from zero in the whole range of λ. Figure 9 shows a peak in Π/M when λ is varied for both levels of approximation. Qualitatively similar behavior in the entropy production was previously observed in the majority vote model exhibiting a singularity at the critical point [5].

Evidently, the accuracy of the plotted estimations (I_5 and I_9) for the entropy production can be improved if we choose larger neighborhood. At the same time the increase of neighborhood is accompanied with technical difficulties in the numerical calculations. Namely, for rare configurations (e.g., fully infected cluster at low values of ρ) the number of the corresponding transitions may be not counted (observed) if the system size (L) is small and/or the sampling time is short.

V. SUMMARY

The present investigations justify that the probability current structure in two-state nonequilibrium lattice systems can be well described by considering only the possible states of a small cluster of sites instead of studying the whole system. If the evolutionary process is controlled by consecutive one-site changes then the corresponding dynamical graph on the n-site cluster is equivalent to an n-dimensional hypercube with edges representing possible transitions between the connected microscopic states. On the analogy of compatibility conditions we have discussed the consequences of graph contraction. This mathematical procedure relates dynamical graphs obtained for different lattice (cluster) sizes. It is demonstrated that the lattice symmetries have significantly influenced the structure of probability currents and can hide the breaking of detailed balance if the analysis is performed on small (symmetric) clusters. Besides it, these investigations help us to identify the microscopic mechanisms destroying the detailed balance. It is found, for example, that the shortest and most relevant probability current loop occurs for four consecutive transitions $[(0,0)\rightarrow(1,0)\rightarrow(1,1)\rightarrow(1,0)\rightarrow(0,0)]$ on two neighboring sites in such a way that both the intensity and direction of this cycle depend on the configuration on the neighboring sites. In the whole system, however, these probability current loops are entangled and yields a complicate probability current structure characterizing the deviations from the detailed balance.

In many cases the deviations from the detailed balance can be quantified by the entropy production. Using the above concepts a simple set of estimations are suggested for the evaluation of the entropy production in nonequilibrium lattice systems in the absence of unidirectional elementary transitions. The application of these approaches is demonstrated by Monte Carlo simulations when studying the two-dimensional contact process with a weak mutation. It is emphasized, however, that the dynamical cluster techniques [14–16] allow us to evaluate analytically all the quantities we need in the evaluation of the entropy production.

The numerical investigations faced us with both the theoretical and technical difficulties. It turned out that the original definition of entropy production is not applicable in a straightforward manner for those dynamical systems where unidirectional transitions occur between two microscopic states (examples are the contact process [19,20], evolutionary games with imitative strategy updates [28,17], and asymmetric exclusion process [27]). On the other hand, the rare elementary events cause technical difficulties in the numerical quantification of transition rates when choosing large cluster.

Finally, we have to mention several general features and possible extensions of the present approach. For example, the dynamical graph consists of Q^M nodes in the Q-state lattice systems of M sites where $s_x=1,\ldots,Q$ for each site x. In addition, the number of edges in the dynamical graph increases significantly if two (or more) neighboring site variables can change simultaneously as it happens for the Kawasaki dynamics [25]. The modifications of the number of states (Q), the dynamics, and the spatial lattice affect the structure of the dynamical graph G including the strength of probability current along the edges of G. Using the above tools in the systematic investigation of the different dynamical graphs one can clarify the relevant and irrelevant differences in the stationary states for a wide scale of nonequilibrium dynamical lattice systems. Evaluating the entropy production we can quantify and study the effect of many microscopic mechanisms on the deviation of detailed balance in nonequilibrium systems of physics, biology, and economics.

ACKNOWLEDGMENTS

We thank Mário J. de Oliveira for useful discussions. This work was supported by the Hungarian National Research Fund (Grant No. 73449).

APPENDIX: GRAPH TOPOLOGY OF HYPERCUBES

Table I summarizes the most relevant topological features of the d-dimensional hypercube.

Most of the quantitative parameters can be checked

TABLE I. Topological parameters of the d-dimensional hyper cube.

Name	Expression
Number of nodes	2^d
Number of edges	$d2^{d-1}$
Degree	d
Number of edges in spanning tree	2^d-1
Number independent loops in KCL	$d2^{d-1}-2^d+1$
Number of four-site loops	$\binom{d}{2}2^{d-2}$

iteratively when creating a $(d+1)$-dimensional hypercube from the d-dimensional one. During this procedure the number of nodes (with all internal edges) is doubled and additionally each new node in the shifted subgraph is linked with its source node. The doubling procedure helps us to define a spanning line that serves to find a possible set of KCL loops.

Notice that the number of four-edge loops is larger than the number of independent current loops we need to introduce for satisfying the KCL. However, only a portion of four-site loops represents elementary process on two nearest-neighboring sites (the actual value is proportional to the number of nearest neighbors in the spatial d-site cluster).

[1] J. Schnakenberg, Rev. Mod. Phys. **48**, 571 (1976).
[2] G. Kirchhoff, Poggendorff's Ann. Phys. Chem. **72**, 495 (1847).
[3] C. Maes, J. Stat. Phys. **95**, 367 (1999).
[4] C. Maes and K. Netočný, J. Stat. Phys. **110**, 269 (2003).
[5] L. Crochik and T. Tomé, Phys. Rev. E **72**, 057103 (2005).
[6] T. Tomé, Braz. J. Phys. **36**, 1285 (2006).
[7] C. Maes, F. Redig, and A. Van Moffart, J. Math. Phys. **41**, 1528 (2000).
[8] P. G. Doyle and L. J. Snell, *Random Walks and Electric Networks* (2000), math.PR/0001057, URL http://arxiv.org/abs/math.PR/0001057
[9] R. K. P. Zia and B. Schmittmann, J. Phys. A **39**, L407 (2006).
[10] R. K. P. Zia and B. Schmittmann, J. Stat. Mech. 2007, P07012.
[11] V. Lecomte, Z. Rácz, and F. van Wijland, J. Stat. Mech. 2005, P02008.
[12] R. Kikuchi, Phys. Rev. **81**, 988 (1951).
[13] T. Morita, J. Math. Phys. **13**, 115 (1972).
[14] H. A. Gutowitz, J. D. Victor, and B. W. Knight, Physica D **28**, 18 (1987).
[15] R. Dickman, Phys. Rev. E **64**, 016124 (2001).
[16] G. Szabó, J. Vukov, and A. Szolnoki, Phys. Rev. E **72**, 047107 (2005).
[17] G. Szabó and G. Fáth, Phys. Rep. **446**, 97 (2007).
[18] B. Andrae, J. Cremer, T. Reichenbach, and E. Frey, Phys. Rev. Lett. **104**, 218102 (2010).
[19] T. M. Liggett, *Interacting Particle Systems* (Springer-Verlag, New York, 1985).
[20] J. Marro and R. Dickman, *Nonequilibrium Phase Transitions in Lattice Models* (Cambridge University Press, Cambridge, England, 1999).
[21] R. J. Glauber, J. Math. Phys. **4**, 294 (1963).
[22] T. Tomé, M. J. de Oliveira, and M. A. Santos, J. Phys. A **24**, 3677 (1991).
[23] M. J. de Oliveira, J. Stat. Phys. **66**, 273 (1992).
[24] M. J. de Oliveira, J. F. F. Mendes, and M. A. Santos, J. Phys. A **26**, 2317 (1993).
[25] K. Kawasaki, in *Phase Transitions and Critical Phenomena*, edited by C. Domb and M. S. Green (Academic Press, London, 1972), Vol. 2, pp. 443–501.
[26] S. Katz, J. L. Lebowitz, and H. Spohn, J. Stat. Phys. **34**, 497 (1984).
[27] B. Derrida, Phys. Rep. **301**, 65 (1998).
[28] M. A. Nowak, *Evolutionary Dynamics: Exploring the Equations of Life* (Harvard University Press, Cambridge, MA, 2006).